

Joint angle coupling of a musculoskeletal model and a graphical model of the hand for enhanced display in medical education

by

J. Cueto Fernández

to obtain the degree of Master of Science at the Delft University of Technology, to be defended publicly on Wednesday August 26, 2020 at 13:30.

Student number: 4742656

Supervisors: Ir. J.E. Geelen, TU Delft

Dr. Ir. W. Mugge,

K. Bogomolova,

Dr. B.P. Hierck,

Prof. Dr. E.C.T van der Helm,

Prof. Dr. S. Hovius,

TU Delft

LUMC

TU Delft

LUMC

An electronic version of this thesis is available at http://repository.tudelft.nl/.





Joint angle coupling of a musculoskeletal model and a graphical model of the hand for enhanced display in medical education

J. Cueto Fernández

Abstract

Advanced anatomical knowledge and understanding of the muscles involved in various movements are crucial for medical practitioners to reach the correct diagnostic and successfully predict surgery outcomes. To acquire this knowledge, 3D graphical anatomical models which are displayed stereoscopically can effectively supplement cadaveric dissections. Nevertheless, the movements implemented in the available graphical models do not accurately reproduce the intricate dynamics of the human body, which is especially relevant in the case of the hand. Biomechanical models, on the other hand, provide accurate movement simulations from experimental data, while lacking a detailed graphical representation. Thus, the current paper focuses on the incorporation of the biomechanical model of the hand developed by Mirakhorlo et al. (2018) into a comprehensive graphical anatomical model (Zygote Media Group Inc), to be used for educational purposes. Motion capture data of a pinch task was acquired to validate the combinational approach, and an inverse kinematics simulation was performed in OpenSim using the musculoskeletal model. A reference value based on the fingertip distance difference at the pinch pose was calculated from the experimental data and the simulated motion by the musculoskeletal This value was used for validation of the musculoskeletal model reproducibility by the graphical model. Comparison shows that the graphical model reproduced the simulated motion with satisfactory visual effects and within an acceptable range from the reference metric. The presented approach is considered a successful first step towards a biomechanically and anatomically accurate graphical model of the human hand. This lays the foundation for further work on minimising the effect of the anatomical differences between the two models in order to achieve a better match.

Keywords Hand model; musculoskeletal model; graphical model; inverse kinematics; motion capture; joints; finger.

1 Introduction

For physical examinations and successful surgeries, medical practitioners need a good understanding of human anatomy and the relationships between structures in the body, such as the effect of antagonistic and synergistic muscles in the generation of movements. This becomes especially relevant in the case of the hand, which is the most complex structure in the human body in terms of motion and accounts for a high percentage of human motor capabilities (Gustus et al., 2012). Nevertheless, several studies have shown that knowledge on the anatomy among undergraduate medical students and recently graduated doctors is insufficient according to experts in the field (Waterston and Stewart, 2005; Bergman et al., 2008).

Acquisition of the required level of anatomical knowledge is facilitated by the traditional cadaveric dissections. Nonetheless, these practices are becoming increasingly scarce due to the costs involved and limited availability of cadavers as well as reduced anatomy teaching time in bachelor educations (Azer and Eizenberg, 2007; Drake et al., 2009). Altogether this translates into two-dimensional (2D) anatomical atlases being the main learning tool for students. This shortage of three-dimensional (3D) anatomy exploration increases the students' difficulty to translate their 2D anatomical knowledge, acquired from books, into the 3D world.

One of the solutions the medical community has proposed to this issue is the use of 3D graphical models for anatomy teaching. These models have proven to be more effective when displayed stereoscopically, i.e. when two offset images are displayed to the eyes, which are then combined by the user's brain to create the perception of depth (Cui et al., 2017; Hackett and Proctor, 2018; Wainman et al., 2018). The benefits derived from this teaching tool are especially relevant for students with low visual-spatial abilities (Bogomolova et al., 2019).

As a result, several 3D graphical models are already available for incorporation into the teaching curriculum, such as Zygote's model of the human anatomy. These models are polygon-based visual representations of the structures in the body, digitized from magnetic resonance imaging (MRI) scans. The anatomical detail and correctness of these models make them a good resource for learning about the structures present in the human body. Nevertheless, only a few of them have movements implemented as an application's feature and, when present, they are always based on visual effects.

These movements thus lack the accuracy to reproduce the complex system of joints, tendons and ligaments present in the human hand.

A promising solution is the incorporation of a biomechanical model into an anatomical graphical model for calculating and displaying of rigorous movements. A biomechanical model is a mathematical algorithm that relates the anatomy to the joint torques through its musculoskeletal model, and ultimately to the force production of the individual muscles by its muscle model and optimisation method. These models can be accompanied by simplistic visual representations in some cases, where muscles are depicted as piecewise lines. Considering this, a biomechanically-enhanced and anatomically detailed graphical model allows for the accurate reproduction of movements, as well as the display of muscle synergism and antagonism by colour coding during movement generation. Additionally, such a combined model could be used to represent clinical scenarios by selective modification of the biomechanical model equations. Some attempts have been made at incorporating biomechanical principles into detailed graphical models (Sachdeva et al., 2015; Tsang et al., 2005), although none of them included a complete biomechanical model. Thus, there is a need for a graphical anatomical model that incorporates a complete and validated biomechanical model.

In this paper, the biomechanical model of the hand developed by Mirakhorlo et al. (2018) was coupled to the graphical model purchased from Zygote Media Group Inc. The used musculoskeletal model is a validated model based on one consistent anatomical data set described in Mirakhorlo et al. (2016), and it was created for its use within the computational software OpenSim (Delp et al., 2007). On the other hand, Zygote's graphical anatomical model must be manipulated using a 3D computer graphics software. Here, Blender (Stichting Blender Foundation, the Netherlands) is the chosen software for the current application due to its open-source nature.

The designed workflow of the biomechanicallyenhanced graphical model comprises the acquisition of motion capture data, which is subsequently processed by the biomechanical model in an inverse kinematics simulation. The result of this process is a progression over time of the calculated individual joint angles that are necessary for the musculoskeletal model to reproduce the recorded motion. These joint angles are subsequently loaded into the graphical model for movement visualisation. This step requires the previous reproduction of the musculoskeletal model joint definitions in the graphical model. Ultimately, the aim of the combined model is to display the biomechanically computed movements in the augmented reality (AR) headset HoloLens (Microsoft Corporation, 2016), as it allows for stereoscopic display to the user and interaction with the model.

The goal of this thesis is reproducing the musculoskeletal model definition in the graphical model, exclusively considering the index and thumb fingers, and validating the combined model's designed pipeline by compliance with an experimentally calculated reference value for the fingertip distance difference between the two models at the pinch position. With this aim, the musculoskeletal model joint configuration was replicated in the graphical model using conventional 3D graphics animation elements and adapted to match its anatomy. A pinch task was recorded using a motion capture system and subjected to the outlined pipeline. Ultimately, the movement was reproduced by the graphical model. This was done in a 2D display as a preliminary step prior to the model's visualisation using a stereoscopic device. The validation of the combinational approach between models was investigated considering an experimentallydefined reference value.

2 Definition of the musculoskeletal model

The biomechanical models developed within the framework of the software OpenSim share a structure that consists of multiple sets. In the model developed by Mirakhorlo et al. (2018) these are: a set of bodies, which correspond to the individual bones or groups of bones (like the carpals); a set of joints connecting these bodies; and a set of actuators, which are the muscles of the hand and forearm.

The model comprises 22 bodies, having the carpal bones grouped as a single segment, and 43 musculotendon units. For each body, the mass of the segment, its inertia tensor and its centre of mass are defined. The muscles are considered as line segments between two viapoints with cylindrical wrapping surfaces at the joints. The muscle model used to calculate muscle forces and activation levels is that developed by Thelen (2003).

The musculoskeletal model accounts for 27 degrees of freedom (DoF), being distributed in the following way: 2 DoF at the joint between the carpal segment and the ulna, to allow for flexion/extension and ulnar/radial deviation; forearm pronation and supination is modelled with 1 DoF at the joint between the ulna and the radius. 1 DoF is allocated at the connection between each of the 2nd to 5th metacarpals¹ and the carpus (carpometacarpal joint), although these joints are locked during simulations. The 1st carpometacarpal joint is an exception and its movement is enabled, consisting of 2 DoF, allowing for flexion/extension and abduction/adduction. The metacarpophalangeal joints of the 2nd to 5th fingers have 2 DoF, while that of the 1st finger has only 1 DoF. All the interphalangeal joints allow for motion along 1 DoF.

Each joint in OpenSim relates the movement of the children body frame to the parent body frame by means

 $^{^1{\}rm The}$ naming convention in an atomy numbers the fingers from 1 to 5 starting at the thumb.

Nomenclature					
Radial styloid	RS	1st metacarpal	MC1		
Ulnar styloid	US	Proximal phalanx of thumb	PP1		
Medial epicondyle	EM	Distal phalanx of thumb	DP1		
Lateral epicondyle	EL	Carpometacarpal joint	CMC		
2nd metacarpal	MC2	Metacarpophalangeal joint	MCP		
Proximal phalanx of index	PP2	Interphalangeal joint	IP		
Medial phalanx of index	MP2	Proximal interphalangeal joint	PIP		
Distal phalanx of index	DP2	Distal interphalangeal joint	DIP		

of a transform matrix. This matrix allows for rotation and translation of the children body with respect to the parent body position and orientation. In the musculoskeletal model of Mirakhorlo et al., the joints are defined as purely rotational, consisting of the combination of a pivot point and one or two rotation axes (depending on the number of DoF of the joint). To achieve translation of the children body frame by a purely rotational motion, the calculated joint pivot points (Mirakhorlo et al., 2016) are located outside of the corresponding anatomical joint surfaces for most of the model joints, as shown in Figure 1a.

3 Methods

3.1 Reproduction of the musculoskeletal model joint definitions in the graphical model

All work performed on the graphical model of the hand anatomy is carried out within the software Blender (version 2.82). This model consists of a set of polygon meshes that shape the bones, muscles, blood vessels, nerves and connective tissue of the hand.

3.1.1 Transfer of the joint pivot points and rotation axes to the graphical model

To relate the graphical and the musculoskeletal models, a common reference frame must be defined. As the two models have different global frames, a consistent local frame based on anatomical landmarks was calculated for both of them. This local frame has its origin at the ulnar styloid (US) landmark, and the axes were established as follows:

- Y: unit vector from the US to the midpoint between the medial and lateral epicondyles (EM and EL) of the humerus.
- Z: unit vector orthogonal to Y and to the vector from the US to the radial styloid (RS).
- X: unit vector orthogonal to Y and Z and pointing in the dorsal direction.

To transfer the coordinates of the anatomical landmarks, joint pivot points and rotation axes unit vectors of the musculoskeletal model data set to the graphical model global frame, the equation used was

$$\boldsymbol{v}_{\mathrm{graph}}^{\mathrm{G}} = (\mathbf{R}^{\mathrm{L} \to \mathrm{G}} \alpha \boldsymbol{v}_{\mathrm{musc}}^{\mathrm{L}}) + \boldsymbol{O}_{\mathrm{graph}}^{\mathrm{G}},$$
 (1)

where $\boldsymbol{v}_{\text{graph}}^{\text{G}}$ are the coordinates of interest transformed to be expressed in the global frame of the graphical model, $\boldsymbol{v}_{\text{musc}}^{\text{L}}$ are the coordinates of interest before the transformation (expressed in the local frame), $\boldsymbol{O}_{\text{graph}}^{\text{G}}$ are the coordinates of the US of the graphical model expressed in its global frame, to account for the translation of the origin. As the real size of the two models differs considerably, the conversion factor α was calculated based on segment length by averaging the individual segments' conversion factor. $\mathbf{R}^{\mathrm{L} \to \mathrm{G}}$ is the rotation matrix used to transform the coordinates from the graphical model's local frame into Blender's global frame and has the form

$$\mathbf{R}^{\mathrm{L}\to\mathrm{G}} = \begin{bmatrix} \mathbf{x}_{\mathrm{graph}}^{\mathrm{L}} & \mathbf{y}_{\mathrm{graph}}^{\mathrm{L}} & \mathbf{z}_{\mathrm{graph}}^{\mathrm{L}} \end{bmatrix}, \tag{2}$$

where $\mathbf{x}_{\text{graph}}^{\text{L}}$, $\mathbf{y}_{\text{graph}}^{\text{L}}$, and $\mathbf{z}_{\text{graph}}^{\text{L}}$ are the local frame axes column vectors calculated using the anatomical landmarks of the graphical model.

Using equation (1), all the anatomical landmarks and joint pivot points were transformed from the musculoskeletal model global frame to the graphical model global frame. Given the differences in anatomy and resting pose between the two models, the joint pivot points must be translated and rotated to match the graphical model. To position a joint pivot point, the head of the anatomical bone that is proximal to the joint of interest is used as the origin of the vector distance to the joint pivot point. Two successive rotations must be applied to correct for any difference in the longitudinal and transversal orientation of the bones between the graphical and musculoskeletal models. For this, the longitudinal orientation of the bone that is proximal to the joint of interest was defined by a unit vector originating at the bone head landmark and pointing to the available immediately proximal landmark (the same bone base landmark or, alternatively, the successive proximal bone head landmark). An example of this is a vector with origin at the head of the medial phalanx of the index (MP2h) and pointing towards the head of the proximal phalanx of the same finger (PP2h). To account for joint transversal orientation differences between models, a unit vector originating at the radial side of the anatomical joint and pointing to the ulnar side was used.

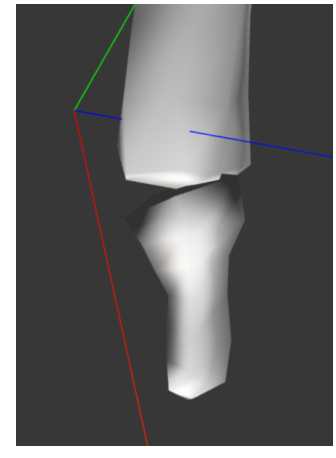
The axis-angle representation of the difference in orientation between the calculated longitudinal vectors of the two models was used to rotate the vector distance defining the position of the joint pivot point relative to the bone head landmark. The transversal orientation vector of the musculoskeletal model corresponding joint must be rotated too. As the longitudinal and transversal orientation vectors are not necessarily orthogonal in the two models, deviations of the already corrected longitudinal orientation when transversally adjusting the joint pivot point position are prevented by projecting the transversal orientation vectors of the two models onto the normal plane to the longitudinal vector. The axis-angle representation of the difference in orientation between the projected vectors was used to rotate the vector distance defining the position of the joint pivot point relative to the bone head landmark. After the joint pivot point orientation has been corrected to adapt to the graphical model bone anatomical orientation, it is translated to the measured anatomical landmark (joint proximal bone head).

The same procedure was applied to the vectors defining the rotation axes of each joint. As these vectors are unit vectors by nature, a modified version of equation (1) was used, excluding the conversion factor and the translation of origin using $O_{\text{graph}}^{\text{G}}$. For the same reason, after subjecting them to the orientation corrections, the rotation axis vectors are not translated to any anatomical landmark.

The process of orientation correction was only applied to the proximal and distal interphalangeal joints of the index (PIP2 and DIP2) and to the metacarpophalangeal and interphalangeal joints of the thumb (MCP1 and IP1), as there is no available data of the transversal orientation of the metacarpophalangeal joint of the index (MCP2) and the carpometacarpal joint of the thumb (CMC1) for the musculoskeletal model. In addition to this, the definition of a longitudinal orientation vector for these joints is misleading, as the anatomy of the palm (composed by the carpals and the 2nd to 5th metacarpals) differs considerably between the two models, as supported by the data presented in the Appendix A.

3.1.2 Definition of the graphical model

Once the joint pivot points have been positioned in the graphical model, a rig must be implemented to enable the movement of the meshes. This rig consists of the so-called armature, which is composed of a set of posebones and the relationships between the meshes and the armature's pose-bones. Each mesh must be parented to





(a) Musculoskeletal model

(b) Graphical model

Figure 1: Comparison of the DIP2 joint pivot point between (a) the musculoskeletal model in OpenSim, represented by the visible 3 axes of the joint frame, and (b) the graphical model in Blender, represented by the highlighted pose-bone.

a pose-bone, being possible to move more than one mesh with the same pose-bone, and a hierarchy between the pose-bones is established. During animation, the visible structures are the meshes, which movement is governed by the rotations applied to the invisible pose-bones to which they are parented.

Pose-bones can only rotate around their base, and thus, to reproduce the joint pivot points from the musculoskeletal model in the graphical model, auxiliary posebones were used for each joint, as depicted in Figure 1b. To prevent the introduction of additional DoF to the graphical anatomical model, the pose-bones passing through the meshes and from the mesh's head landmark to the joint pivot point are merely structural and the junctions between them were locked at all times. Rotations are only applied to the pose-bones joining the joint pivot point and the immediately distal mesh's base landmark (such as that highlighted in Figure 1b), reproducing the configuration of the musculoskeletal model.

The defined rig configuration, consists of one independent pose-bone for the ulna as the highest pose-bone in the hierarchy, which is not physically connected to any other and is static. Another pose-bone is assigned to the radius, which is parented to the ulna pose-bone, in order to eventually allow for pronation and supination by rotating around the ulna. Although this movement was considered when building the armature, forearm pronation-supination is out of the scope of this thesis and thus, this joint is locked and was not defined in accordance to the musculoskeletal model definition. Extruded from the radius pose-bone, there is the pose-bone to which the eight carpal bones are parented, as these are considered as a single body in the musculoskeletal model. Parented to this pose-bone, there are the pose-bone for

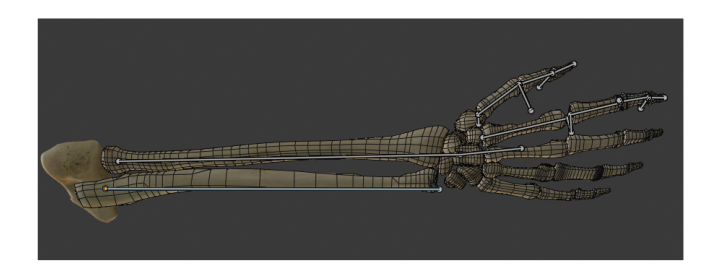


Figure 2: Armature built to rotate the graphical model's mesh bones using the same definition of the joint pivot points and rotation axes of the musculoskeletal model. The pose-bones of the rig are represented by the grey rods. Moreover, the grey spheres represent the junctions between pose-bones.

the 2nd metacarpal and the auxiliary pose-bone of the 1st metacarpal. As the joint between the carpals and the 2nd metacarpal is locked in the musculoskeletal model, this pose-bone is simply parented to the carpals and its distance and orientation with respect to the carpals is kept constant during movement. The auxiliary pose-bone of the CMC1 joint has its head at the transferred joint pivot point from the musculoskeletal model and its tail at the base of the 1st metacarpal (MC1b). 16 pose-bones are successively extruded from the last two cited pose-bones, using auxiliary pose-bones to match the anatomically corrected joint pivot point locations from the musculoskeletal model for the joints MCP1, IP1, MCP2, PIP2 and DIP2. The structure of the armature is depicted in Figure 2.

3.2 Motion capture of a pinch task

A pinch task was chosen for validating the transfer of the joint pivot points and rotation axes from the musculoskeletal model to the graphical model. This decision was based on the potential of the pinch task for allowing the use of clear metrics of movement reproducibility and on the movement complexity, which makes it a good indicator of the capability to model intricate movements.

Several repetitions of the pinch task were recorded using a motion capture system (Oqus 7 from Qualisys (Götenburg, Sweden)) comprised of 12 cameras. Reflective markers of 12 mm in diameter were attached to the participant's hand. The markers were placed at the following landmarks: US, RS, EM, EL, MC2h, PP2h, MP2h, DP2h (or index fingertip), MC1b, MC1h, PP1h, DP1h (or thumb fingertip). One additional marker was placed at the fingertip of each of the 3rd to 5th fingers to keep track of their position for assessment during the posterior data processing. Figure 3 shows the used marker configuration.

Fingers 3 to 5 were immobilised and the participant's wrist was maintained as still as possible during the pinch task. The position of the shoulder was 90° abducted from the standard anatomical position and the elbow,

90° flexed. This configuration was chosen to achieve a pose that could be recorded by the camera set, avoiding marker occlusion, and that would maintain a neutral position for the elbow supination-pronation. Three recordings of 10 seconds each were performed and a total of six pinch task repetitions performed at different speeds were filmed.

3.3 Scaling of the musculoskeletal model and inverse kinematics simulation

Inverse kinematics (IK) was used to calculate the joint angles over time necessary to achieve the recorded pinch task motion. The musculoskeletal model was first scaled to match the experimental data set. The scaling process was carried out with the aid of the computational software OpenSim (version 4.1). Manual scaling, which consists in calculating the individual scale factors that must be applied to each segment, was conducted. A segment is represented by a pair of markers, and the difference in distance between the experimental markers pair and the virtual markers equivalent is used to compute the scaling factor. The model was scaled to match the experimental data sets from the three recordings and a different set of scaling factors for each data set resulted from this process. The averaged scaling factors are reported in Table 1 The muscles and the mass and inertial properties of the model were also scaled according to these factors, as well as the model geometries used for a simplified visualisation within the software OpenSim.

Subsequently, the musculoskeletal model static pose was calculated to match that of the experimental data. Additionally, the virtual markers of the model were moved to match the position of the experimental markers in the static pose. The procedure for this is to compute the generalised coordinates that minimise the error between experimental and virtual markers for a small set of time steps. The set of generalised coordinates for each time step is calculated by solving the following weighted least squares equation (SimTK Confluence.



Figure 3: Marker configuration used with the motion capture system to record the pinch tasks. Markers at the EM and EL landmarks are not visible in the image, but were present during the recordings.

Stanford University, c)

$$\min_{\boldsymbol{q}} \left[\sum_{i \in \text{markers}} w_i \left\| \boldsymbol{m}_i^* - \boldsymbol{m}_i(\boldsymbol{q}) \right\|^2 \right], \quad (3)$$

where q is the generalised coordinates vector being solved for, m_i^* is the position of the experimental marker i and $m_i(q)$ is the position of the corresponding virtual marker in the model, which is dependent on the coordinate value. Locked coordinates are not considered during the calculations, and their value is kept as the prescribed one. The marker weight w_i must be specified for each marker, in order to weight lower markers whose position might have a large variability and weight higher those which position is more reliable. For the calculation of the static pose and marker positioning, the markers located at the fingertips of the index and thumb were weighted ten times higher than the rest.

Consecutively, the inverse kinematics simulation was computed in OpenSim. This was calculated by solving the least squares problem described by equation (3) for the entire duration of the experimental data this time. All markers were weighted equally for the inverse kinematics problem, being the elbow translation and rotation locked during the calculations. The IK problem was solved for the three recorded data sets, resulting in the sets of joint angles necessary to reproduce the six repetitions of the pinch task.

The marker errors were independently calculated for the scaling and static pose computation combined step and for the IK simulation. The reported errors were the total squared error, the Root Mean Squared Error (RMSE) and the maximum marker error.

For the recorded six pinch task repetitions, the position over time of the markers located at the fingertips were documented during the entire simulation for their posterior analysis.

3.4 Correction of the graphical model resting pose to match that of the musculoskeletal model

As the result of the inverse kinematics simulation is a set of joint angles, which must be rotated over the corresponding rotation axis and at the adequate pivot point for each joint, the resting pose of the musculoskeletal model and the graphical model must be coincident in order to attain the same physical rotation in the two models. The resting pose of the graphical model was modified in Blender to match that of the musculoskeletal model, as the simulation angles are calculated with respect to the model's resting pose in OpenSim.

It must be noted that the angles of the joints of the musculoskeletal model at the resting pose are considered as the zero angles, but these are not necessarily coincident with those at the standard anatomical position of the hand. Thus, the angle between the proximal and distal segments to each joint were compared in the graph-

Table 1: Averaged scaling factors used to scale the musculoskeletal model for inverse kinematics simulation, computed using the three recorded data sets. The standard deviation (SD) are also reported. The segments of the fingers 3 to 5 were scaled using the same scaling factors as the index finger for consistency, as there was no available data of their segments length.

Segment	Scaling factor		
Ulna	$0.9970 \pm 0.0038 \text{ SD}$		
Radius	$1.0111 \pm 0.0083 \text{ SD}$		
Carpals	$1.0000 \pm 0.0000 \text{ SD}$		
1^{st} metacarpal	$1.1960 \pm 0.0442 \text{ SD}$		
Proximal phalanx 1	$0.8630 \pm 0.0341 \text{ SD}$		
Distal phalanx 1	$1.2149 \pm 0.1128 \text{ SD}$		
2 nd metacarpal	$1.0000 \pm 0.0000 \text{ SD}$		
Proximal phalanx 2	$0.9277 \pm 0.0031 \text{ SD}$		
Medial phalanx 2	$0.7883 \pm 0.0388 \text{ SD}$		
Distal phalanx 2	$1.1164 \pm 0.0269 \text{ SD}$		

ical model to the musculoskeletal model and adapted. The followed protocol was calculating the angle between the vectors drawn from the joint pivot point which angle is being assessed to the proximal and distal consecutive joints or landmarks. The joints and landmarks used to define the angle of each joint are listed in Table 2.

For each joint with 1 DoF, the proximal and distal vectors were normalised and the angle between their projections on the plane which normal is the corresponding joint's rotation axis was calculated. The difference in this angle between the musculoskeletal and graphical models was used to rotate the corresponding joint in the graphical model by the calculated angle over its rotation axis. For joints with 2 DoF, a second successive correction was done over the remaining rotation axis.

The correction of the resting pose joint angles was successful for all the considered joints excluding the CMC1 and MCP2. The anatomical differences between the two models at the level of the palm (carpals and metacarpals 2 to 5) generated dissimilar resting pose configurations, which caused the need for correcting these angles by visual inspection of the two models. These anatomical discrepancies and their consequences are further described in Appendix A. The chosen angles for the CMC1 joint were 6.00° adduction and 7.50° flexion. The angles set at the MCP2 joint were 7.50° abduction and 5.73° flexion.

Additionally, a difference in the index and thumb transversal orientation was observed. This was corrected by rotating the fingers of the graphical model to match the orientation of those of the musculoskeletal model. The difference between the angles of the two models MCP1 and PIP2 joints transversal vectors was calculated by projecting these vectors on the planes which

Table 2: Segment definition for correction of the resting pose between models.

Joint being evaluated	Joint pivot points or landmarks defining the proximal segment	Joint pivot points or landmarks defining the distal segment
Wrist	US to wrist	Wrist to MCP2
CMC1	Wrist to CMC1	CMC1 to MCP1
MCP1	CMC1 to MCP1	MCP1 to IP1
IP1	MCP1 to IP1	IP1 to DP1h
MCP2	Wrist to MCP2	MCP2 to PIP2
PIP2	MCP2 to PIP2	PIP2 to DIP2
DIP2	PIP2 to DIP2	DIP2 to DP2h

normal vectors are the longitudinal vector of the 1st metacarpal and the proximal phalanx of the index, respectively. The thumb was rotated according to the calculated angle of -45.58° at the CMC1 joint, over the axis generated at the MC1h and with the direction of the longitudinal orientation of the 1st metacarpal of the graphical model. The index was rotated at the MCP2 joint by and angle of -10.45° over the axis established from the PP2h and following the direction of the longitudinal orientation of the index proximal phalanx. These transversal rotations of the entire fingers were calculated and applied prior to the individual joint angles adjustment.

The graphical model in the corrected resting pose is depicted in Figure 4 besides the musculoskeletal model, for visual comparison of the two resting poses.

3.5 Reproduction of the calculated joint angles in the musculoskeletal model by the graphical model

To achieve the recorded movement using the graphical model, its joints must be operated using a sequence of angles which must be rotated along the corresponding rotation axis and at the corresponding joint's pivot point. As a consequence of the internal functioning of the software Blender, the designed protocol for rotating each joint consists in transforming the corresponding rotation axis from the global frame of the graphical model to the local frame of the auxiliary pose-bone, which is intrinsic to Blender architecture. To achieve this, two successive transformations are performed, using the transform matrices of the armature as a whole and of the pose-bone of interest. Once the rotation axis is defined in the corresponding pose-bone local frame, the combination of axis and angle is converted into a quaternion and applied to the pose-bone to achieve the desired rotation. This is done using the formula

$$q* = \begin{pmatrix} \cos(\frac{\beta}{2}) \\ x\sin(\frac{\beta}{2}) \\ y\sin(\frac{\beta}{2}) \\ z\sin(\frac{\beta}{2}) \end{pmatrix}, \tag{4}$$

where q* is the quaternion, β is the angle to be rotated and $x,\ y,\ z$ are the coordinates of the rotation axis in the pose-bone local frame. The transformations between rotation conventions were calculated according to the definition used in the Robotics System Toolbox of MATLAB (2020a). The rotations defined in the form of quaternions were applied to the pose-bones through Blender's application programming interface (API), using the Mathutils module.

The angle of rotation of each of the seven consid-

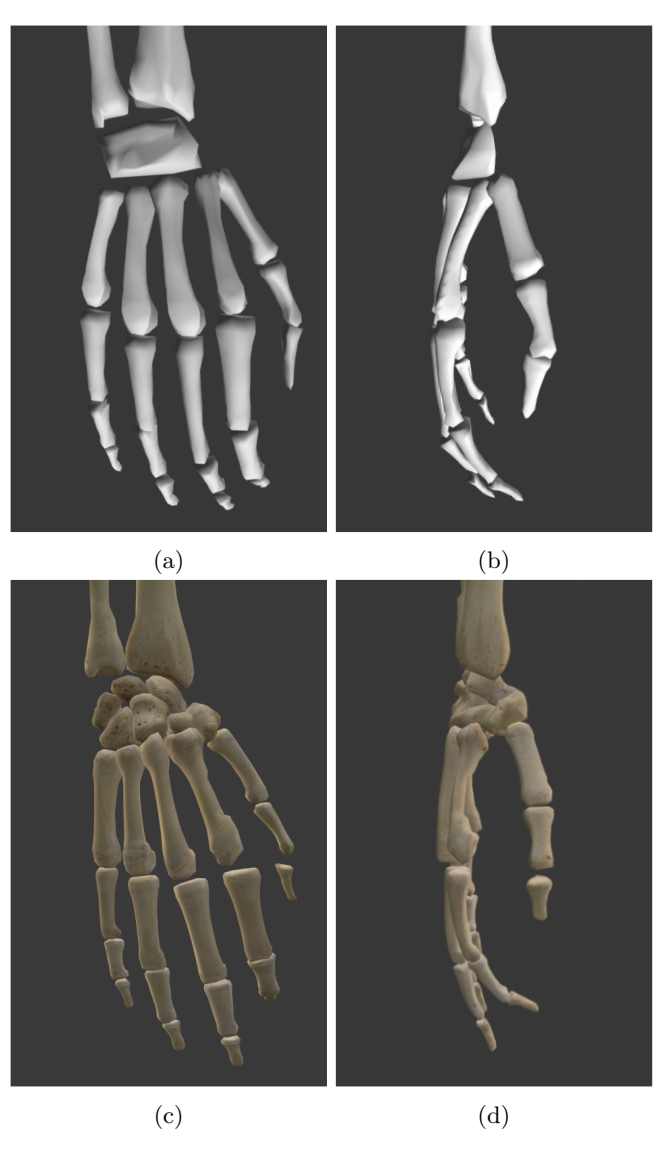


Figure 4: Resting pose of the musculoskeletal model and equivalent corrected resting pose of the graphical model, visualised from two different perspectives. Only the wrist, index and thumb fingers were adjusted.

ered joints is adjusted for each time step using the set of angles exported from OpenSim. To account for the correction of the graphical model resting pose, the corresponding exported rotations from OpenSim (one or two depending on the number of DoF of the joint) are multiplied in the form of rotation matrices to that used to set the joint angle at the adjusted resting pose. This product of rotation matrices is then transformed into a single quaternion, by which the corresponding pose-bone is rotated and keyframed² at each time step.

The rotation matrix used for the joints with 2 DoF has the same definition as that intrinsic to the CustomJoint developed for OpenSim musculoskeletal models (Seth et al., 2010). The transform matrices used for these joints in OpenSim are designed to account for combined rotation and translation along specified axes. As the definition of the current musculoskeletal model is based on pure rotation, the part of the CustomJoint transform matrix that accounts for rotation of the joints with more than one DoF can be simplified to the product of the matrices used to define the rotation over each of the axes individually. Thus, in the cases in which the joints must be rotated over two different axes in the graphical model, the desired motion was achieved by the product of the two individual rotation matrices and the one used to correct the resting pose.

The coordinates of the index and thumb fingertips of the graphical model, as defined in the musculoskeletal model, were extracted for each time step during the animation of the model. These coordinates were reported in the global frame of the graphical model for the six repetitions of the pinch task.

3.6 Analysis methodology

To validate the reproduction of the musculoskeletal model configuration in the graphical model, the index and thumb fingertip coordinates of the two models and the experimental data were assessed. To compare the coordinate sets, these were transformed to be expressed in the corresponding local frames with origin at the US. In addition to this, the coordinates of the graphical model were scaled using the conversion factor α from equation (1).

To calculate the metric chosen as the reference value for validation, the distance between the index and thumb fingertips at the pinch position, where it is minimised, was calculated. This value is normalised by the initial fingertip distance, in order to account for possible anatomical differences between the models, which will reflect in the distance between the index and thumb at the starting position. The metric was calculated as

$$d_{i} = \|(x_{i} \ y_{i} \ z_{i})_{\text{thumb}} - (x'_{i} \ y'_{i} \ z'_{i})_{\text{index}}\|,$$
 (5)

where d_i is the distance between fingertips in meters at a specific time step, and $(x_i \ y_i \ z_i)_{\text{thumb}}$ and $(x_i' \ y_i' \ z_i')_{\text{index}}$ are the fingertip coordinates at the specified time frame. This distance is then normalised as d_i/d_0 , being d_0 the fingertip distance at the initial position. This normalisation enables the comparison of the proportional distance between the fingertips at the pinch pose with respect to the initial distance, between the recorded experimental data, the musculoskeletal model, and the graphical model.

To determine the reference value for acceptable results, the difference between the aforementioned metric calculated for the experimental data set and for the musculoskeletal model after scaling and IK was computed as

Reference =
$$\left\| \frac{d_{\min}^{\text{exp}}}{d_0^{\text{exp}}} - \frac{d_{\min}^{\text{musc}}}{d_0^{\text{musc}}} \right\|$$
, (6)

where d_{\min}^{\exp} and d_0^{\exp} are the distance between fingertips in the experimental motion capture data at the pinch position and at the initial pose respectively. d_{\min}^{\max} and d_0^{\max} are the equivalent measurements for the scaled musculoskeletal model.

This metric was considered as the acceptance level as during the scaling and IK calculations the fitting of the musculoskeletal model virtual markers to the experimental markers was within the acceptable outcome as defined in the software documentation (SimTK Confluence. Stanford University, a,b), meaning that the musculoskeletal model reproduces the experimentally recorded motion with an acceptable level of accuracy. This entails an error threshold of 2 cm for the maximum marker error. The reported errors during the simulation of the six pinch tasks were kept below this value, with the only exception of exceeding this threshold by 0.1 cm at the scaling and static pose calculation combined step for repetitions 1 to 3 of the pinch task (which were recorded in the same data set). Despite of surpassing the maximum marker error limit, the metric can be considered as adequate, as the higher weighting of the fingertip markers during the scaling and static pose computation step accounts for a smaller error at these markers, which are the ones used to calculate the reference value of equation (6). Additionally, this metric accounts for the anatomical differences between the scaled model and the hand of the participant for which the motion capture was recorded.

The same metric from equation (6) was calculated for the difference between the graphical model and the scaled musculoskeletal model. To consider the reproduction of the musculoskeletal model by the graphical model as validated, this metric should be within the range of the computed reference value.

The normalised fingertip distance was calculated for the entire duration of each data set for the experimental markers, the musculoskeletal model and the graphical

²Keyframing is an animation technique which consists in setting a representative attribute of the structures being animated to certain values at specific time points or frames. In this case, the keyframed attribute is the orientation of the pose-bone.

model. The RMSE and correlation coefficient were calculated for the experimental data with respect to the scaled musculoskeletal model, and, separately, for the graphical model with respect to the scaled musculoskeletal model.

All the aforementioned metrics were averaged over the six repetitions of the pinch task and the corresponding standard deviation (SD) values were calculated.

To evaluate the effect of the scaling of the musculoskeletal model in the reference and validation metrics, the already simulated kinematics were run in the unscaled musculoskeletal model. The same measurements were performed for the unscaled musculoskeletal model with respect to the experimental data and the graphical model.

4 Results

4.1 Operative graphical model able to reproduce the joint definitions of the musculoskeletal model

To visually test the correct transfer of the joint pivot points and rotation axes from the musculoskeletal model to the graphical model, the latter was set in three poses where different joints were rotated (Figure 5). These poses consisted in 45° of flexion applied to all the joints of the fingers, as well as 20° of abduction for the joints with 2 DoF. The wrist was set to 45° of flexion, in addition to 20° of adduction. Joint rotations in the correct anatomical directions were attained and visual similarity with the unscaled musculoskeletal model was observed.

Some non-anatomically correct translation of the bone meshes is derived from the purely rotational motion applied at the pivot points of the joints. This translation was originally present in the musculoskeletal model, and thus it does not imply a failure at replicating the model configuration.

4.2 Results of the inverse kinematics simulation from motion capture

The motion generated by the solved generalised coordinates (joint angles) using IK is displayed in Videos 1 and 2 of the Supplementary Material. The total squared error reported for the step involving scaling and setting of the static pose was of 0.0017 m for repetitions 1 to 3 of the pinch task. The computed RMSE of the markers was 0.0118 m, being the maximum marker error achieved at the MCP1 marker (located at the anatomical landmark corresponding to the head of the 1st metacarpal) with a value of 0.0210 m. The total squared error for pinch trials 4 and 5 was of 0.0012 m, and the markers RMSE was 0.0101 m. The maximum marker error was attained at the US and had a value of 0.0176 m. Regarding the last

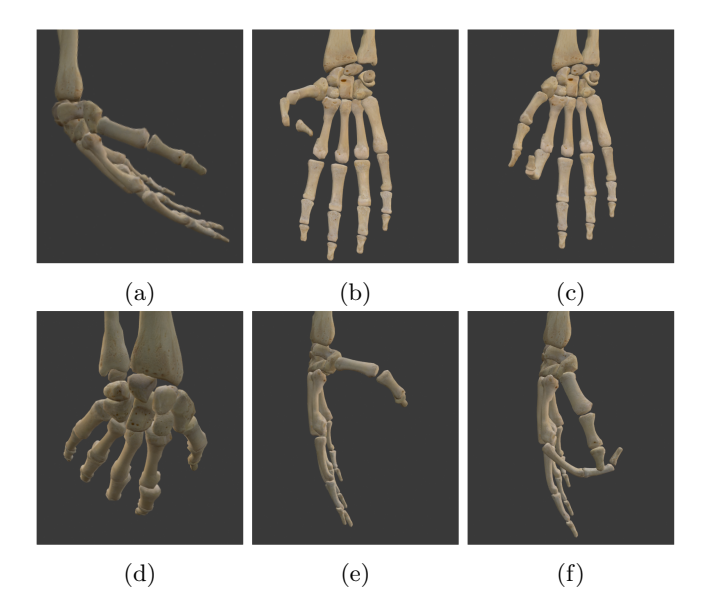


Figure 5: Testing of the anatomically correct rotation direction of the joints in the graphical model: (a) and (d) show 45° flexion and 20° adduction of the wrist from two different perspectives; (b) and (e) show 45° flexion and 20° abduction of the CMC1 and 45° flexion of the MCP1 and IP1 from two different perspectives; (c) and (f) show 45° flexion and 20° abduction of the MCP2 and 45° flexion of the PIP2 and DIP2 from two different perspectives.

pinch task repetition, the total squared error was 0.0011 m and the markers RMSE, 0.0099 m. The maximum marker error was again found at the US with a value of 0.0175 m. The error measurements for each time step of the inverse kinematics simulation of the six pinch task repetitions were also calculated by the software, being all of them well below the 2 cm threshold. This shows that the experimentally recorded motion capture data was successfully reproduced by the musculoskeletal model after scaling.

The chosen metrics were computed for the fingertip coordinates of the index and thumb of the scaled musculoskeletal model during the simulation of the motion. The individual reference values, RMSE and correlation coefficients computed for the six pinch task repetitions are reported in Table 3. The computed average reference value for validation was 0.0166 ± 0.0106 SD. The RMSE between the normalised fingertip distance over time for the experimental data and the scaled musculoskeletal model, averaged over the six task trials, was 0.0191 ± 0.0042 SD and the correlation coefficient, 0.9992 ± 0.0002 SD.

The averaged reference value when running the computed kinematics using the scaled musculoskeletal model in the unscaled one was 0.0637 ± 0.0200 SD. The RMSE and correlation coefficient between the unscaled musculoskeletal model and the experimental data were 0.0373 ± 0.0058 SD and 0.9986 ± 0.0005 SD, respectively.

4.3 Results of movement reproducibility by the graphical model

The resulting joint angle values over time from the IK simulation performed with the musculoskeletal model were applied to the graphical model and an animation reproducing the movements was generated. This can be seen in Videos 3 and 4 of the Supplementary Material. A comparative image of the graphical model and the scaled musculoskeletal model at the pinch position attaining the shortest fingertip distance in the pinch repetition number 1 is depicted in Figure 6 for visual comparison.

The chosen metrics were computed for the fingertip coordinates of the index and thumb of the graphical model during the reproduction of the motion for the six independent pinch task repetitions. These are reported in Table 3. The averaged validation metric (difference in normalised fingertip distance at the pinch pose between the graphical model and the scaled musculoskeletal model) was 0.0196 ± 0.0114 SD. The RMSE between the normalised fingertip distance over time for the graphical model and the scaled musculoskeletal model, averaged over the six pinch trials, was 0.0395 ± 0.0164 SD. The average correlation coefficient was found to be 0.9972 ± 0.0013 SD. The evolution over time of the normalised fingertip distance of the graphical model, the scaled musculoskeletal model and the experimental data can be seen in Figure 7 for the six pinch task repetitions.

5 Discussion

The configuration of the musculoskeletal model developed by Mirakhorlo et al. (2018) was reproduced in the graphical model (Zygote Media Group Inc) and adjusted to the model anatomy. To validate the transfer of joint pivot points and rotation axes, motion capture recordings of a pinch task were used to set a reference value for the maximum allowed difference between the musculoskeletal model kinematics and the graphical model outcome. The chosen metric was the difference in the normalised fingertip distance at the pinch position between the experimental data and the musculoskeletal model (reference value) and between the latter and the graphical model (validation metric). The presented approach succeeds in combining the two models, generating a biomechanically-based graphical model that can be used in medical education. Further improvements are needed in several aspects, considering the work presented in this paper as a successful first combinational attempt between the two models.

The pivot points and rotation axes of joints CMC1 and MCP2 were not corrected based on the longitudinal and transversal orientation differences between the graphical and the musculoskeletal models. This was due to the lack of the necessary landmarks to correct these joints in the anatomical data set of the musculoskeletal model (CMC1 ulnar and radial landmarks, MC2b and

MCP2 ulnar and radial landmarks). Attempts at using the RS for longitudinal orientation correction were made, but these were deemed imprecise, considering the differences in the palm dimensions between the two models and in the resting pose.

Manually adjusting the CMC1 and MCP2 angles in the graphical model to match the musculoskeletal model resting pose is not ideal and might introduce some inaccuracies, which could reflect in the fingertip trajectories. Multiple automatisation approaches were tested, failing always to reproduce the musculoskeletal model resting pose at these joints due to the differences in the hand anatomy. The difference in dimensions of the palm (carpals and 2nd to 5th metacarpals) between the models, as measured by the angle between the lines originating at the RS and ending at the MC2h and MC1b landmarks, accounts for an angle difference of 8.69°. This is within the range of the necessary angles to adjust the resting pose, and thus it influences the correcting approach. In addition to this, the difference in the transversal orientation of the joints between models is not constant for the joints belonging to the same finger, which affects the results of the designed resting pose correction algorithm. All these anatomical differences are further described in Appendix A. An optimisation algorithm based on a least squares problem that would compute a resting pose angle for these specific joints which minimises the differences between models at the resting position could be developed in the future to improve the matching.

Non-anatomically correct gaps can be observed at some joints in the graphical model during movements. These were also present in the musculoskeletal model, and thus they were expected to happen in the graphical model. As part of the future work, relating the purely rotational motion of the musculoskeletal model and new joint kinematics involving rotation and translation in the graphical model that would eliminate the gaps during movement could be assessed, always subjected to critical evaluation by hand anatomy experts.

The computed maximum marker error during scaling of the musculoskeletal model and setting of the static pose overcame the 2 cm threshold by 0.1 cm for repetitions 1 to 3 of the pinch task, and, although lower than the threshold, was in the same range for the remaining repetitions. In spite of considering this 2cm threshold as an acceptable result as stated in the software documentation, it can be deemed a relatively large difference for the case of the hand, which focuses on a smaller scale than gait analyses for example. Attempts were made to minimise this error by weight tuning of the markers, resulting in no better outcomes than the one presented in this paper. Some limitations regarding the acquisition of the experimental data were identified. To accurately determine a segment position and orientation in 3D, at least three non-collinear markers are needed. Given the small dimensions of the human hand

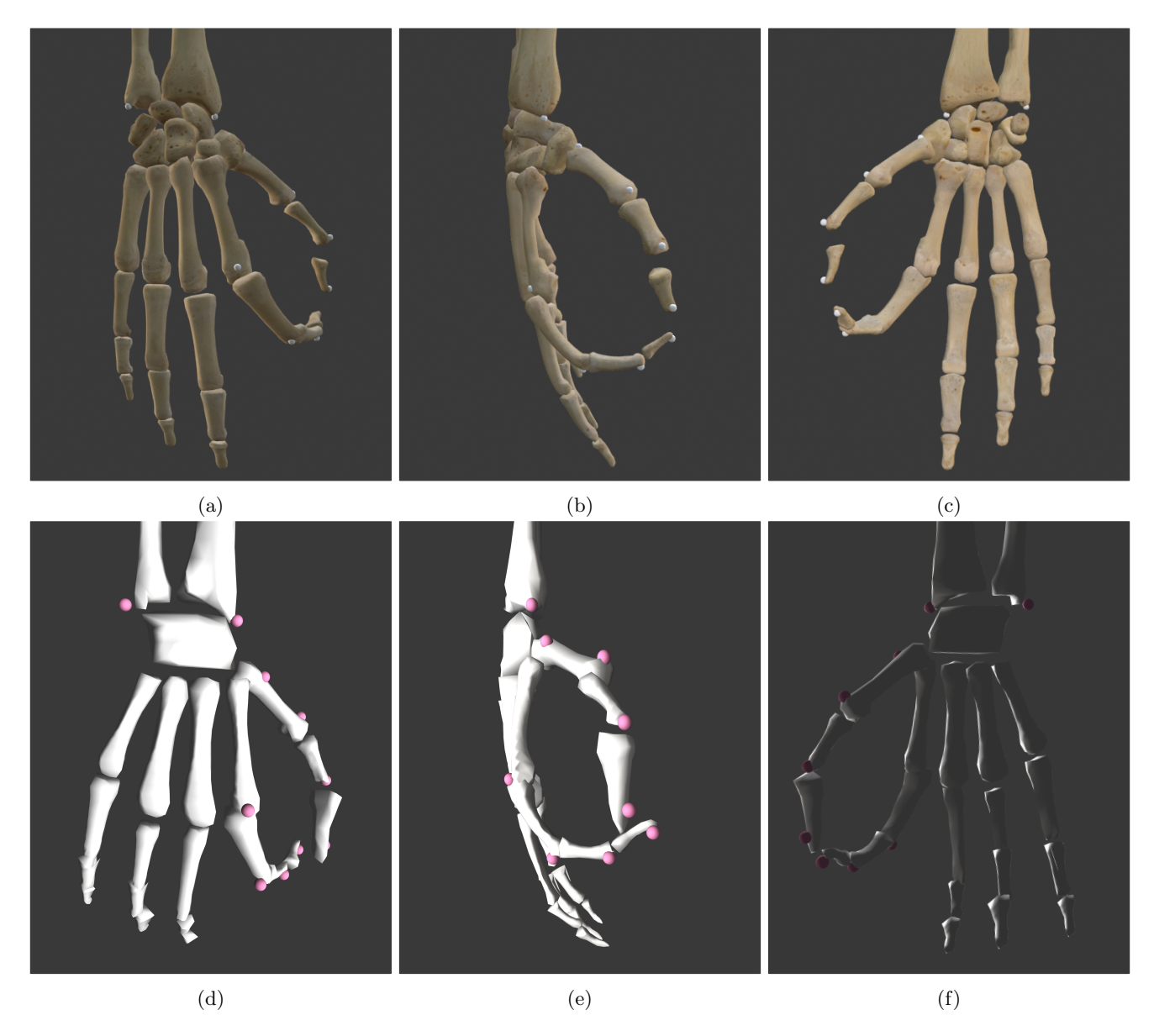


Figure 6: Visual comparison of the scaled musculoskeletal model and the graphical model at the pinch position in repetition number 1, shown from three different perspectives. The pink and light grey spheres represent the virtual markers. Some visual artifacts are generated in the musculoskeletal model display in OpenSim during the scaling process which might difficult the visual assessment of the motion. For this reason, the markers are displayed in the original anatomical landmarks. (f) is shown in a darker shade due to the lighting settings for display in OpenSim, which could not be modified.

Table 3: Computed metrics for the scaled musculoskeletal model, graphical model and experimental data for each of the six pinch task repetitions.

	Rep. 1	Rep. 2	Rep. 3	Rep. 4	Rep. 5	Rep. 6
Reference value	0.0195	0.0340	0.0032	0.0174	0.0174	0.0082
$egin{array}{c} ext{Validation} \ ext{metric} \end{array}$	0.0156	0.0111	0.0233	0.0270	0.0047	0.0361
RMSE (exp. data to scaled musc. model)	0.0173	0.0183	0.0229	0.0161	0.0268	0.0152
RMSE (scaled musc. model to graphical model)	0.0639	0.0224	0.0466	0.0470	0.0355	0.0214
Correlation coefficient (exp. data to scaled musc. model)	0.9991	0.9990	0.9991	0.9994	0.9993	0.9993
Correlation coefficient (scaled musc. model to graphical model)	0.9956	0.9985	0.9958	0.9975	0.9971	0.9986

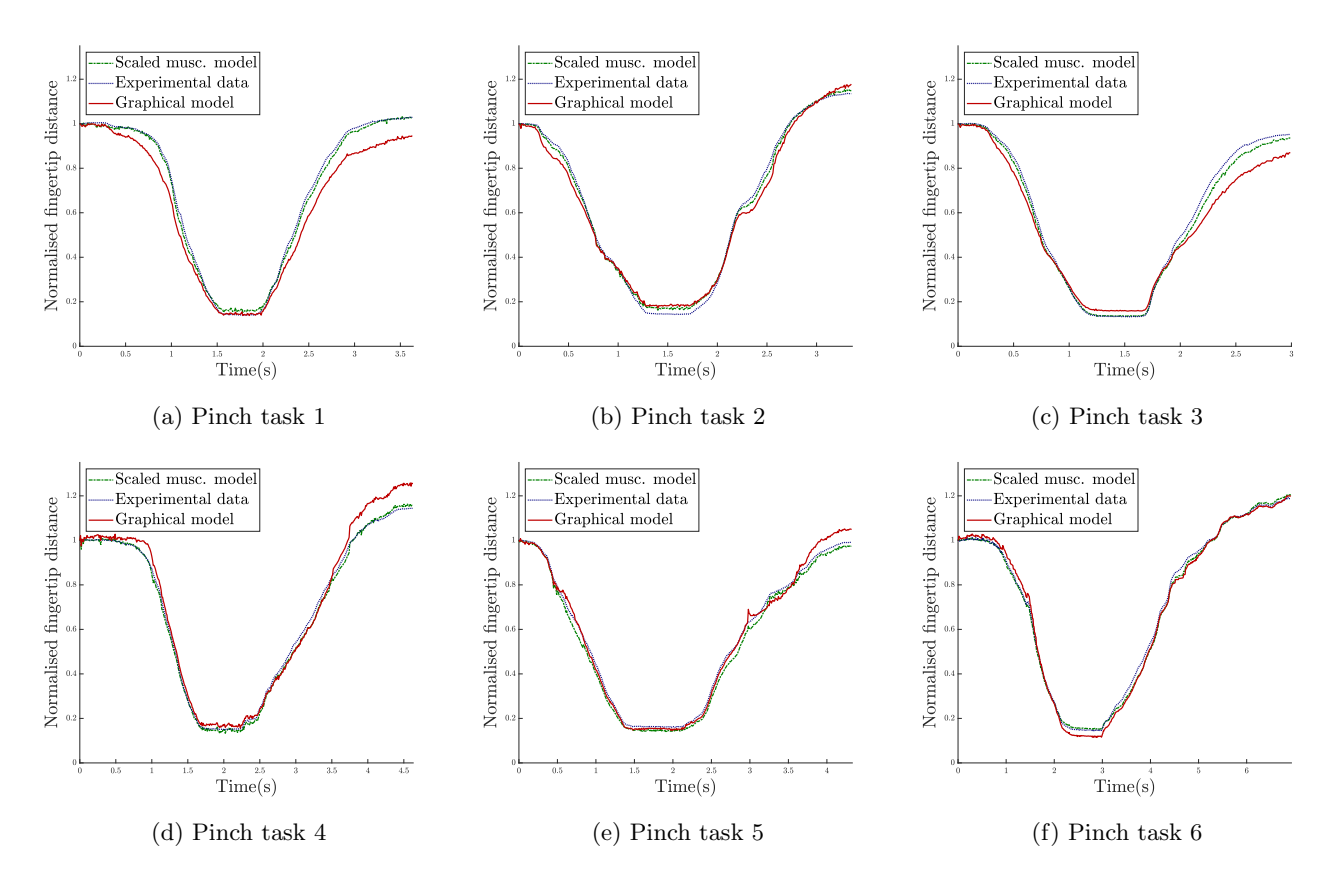


Figure 7: Normalised fingertip distance over time of the scaled musculoskeletal model, the graphical model and the experimental data, displayed for each of the six pinch task repetitions.

and the available motion capture equipment, this was infeasible, as smaller markers were not properly recorded by the equipment. Increasing the number of markers per segment with the used marker size was also found to be inaccurate due to the motion capture system software failing to differentiate individual marker trajectories and generating marker jumps throughout the motion. Moreover, due to unforeseen and uncontrollable circumstances³, it was not possible to perform additional motion capture recordings, nor measurements in more participants, being the author the only participant. The small number of available experimental data sets, all belonging to a single participant, limited the analysis of the results, as well as making the comparison between different anatomies not possible. The reported marker error can thus be explained by the use of a reduced marker set and possible artifacts introduced by skin movement. Additionally, some differences in the rotation axis of certain joints of the thumb were noticed between the musculoskeletal model and the recorded data, which could also influence the model fitting to the experimental data. The reader is directed to Appendix B for a more comprehensive discussion on this. The non-zero value of the used reference metric for validation of the movement reproducibility by the graphical model is thus explained by these constraints. In spite of the discussed limitations and the computed errors for some markers being in the range of 2 cm, the fingertip position error was dampened by weighting the markers at the index and thumb tips higher, penalising the error in their position. As the fingertip coordinates are the ones used to compute the reference and validation metrics, the current approach for the validation of the movement reproducibility by the graphical model can be considered as reliable. In future work, the use of additional recording equipment with more tracking cues could improve the fitting by providing a more extensive marker set for the calculations.

Hyperextension can be noticed in some joints during the movements provided in Videos 1 to 4 of the Supplementary Material. This motion was also present in the recorded experimental data and, again, is caused by the limitation imposed on the participants anatomy, being the only included participant able of naturally performing this hyperextension.

The differences in the fingertip distance between the scaled musculoskeletal and graphical models arise from their anatomical differences. This is analysed in depth in Appendix A. By scaling the musculoskeletal model to the experimental data set, the proportions of their segments become more similar, which reduces the error between the normalised fingertip distance at the pinch

position (reference value). The lack of scaling of the graphical model introduces different proportions of the finger segments and palm dimensions. These differences reflect in the computed validation metric, as fingers with different phalanges proportions, that are flexed at the same angles, attain different endpoint positions. This, together with the variation in the palm dimensions account for a validation metric that is higher than the computed reference value. Nevertheless, as can be observed in Figure 7, the normalised fingertip distance over time of the scaled musculoskeletal model, the graphical model and the experimental data followed a similar pattern for all the pinch task repetitions, which further supports the satisfactory visual results. The computed validation metric was also within the range of the reference value, which signals a remarkable fitting of the graphical model to the scaled musculoskeletal model given that no scaling has been applied to the graphical model. Additionally, different non-normalised initial fingertip distance in the graphical and scaled musculoskeletal models were observed, as well as different spanned distances during movement simulation. This made the normalisation of the validation metric necessary in order to compare the proportional fingertip distance variation in the two models.

The effect of scaling the models can be noticed by considering the reference metric computed using the fingertip data from the unscaled musculoskeletal model. This reference value is considerably higher than the one calculated for the scaled musculoskeletal model, and is also higher than the validation metric between the scaled musculoskeletal and the graphical models, pointing at the importance of scaling for an improved model fitting. In future work, segment-specific scaling of the graphical model should be considered, in order to match the anatomy of the musculoskeletal model. Nevertheless, complications due to Blender definition of meshes will arise from such approach when considering the remaining structures in the graphical model, such as muscles and connective tissue, which would need to be scaled as well

The observed differences in the fitting between the scaled musculoskeletal model, the graphical model and the experimental data for the different pinch task repetitions are due to the different combination of joint angles. Given the small sample size of this thesis, it was not possible to extract any conclusive relationship between joint angles combination and the reference and validation metrics. Further work should include the recording of a larger sample size.

Future directions

Future directions in the project pipeline should consider, besides the already proposed improvements, the addition of a rig for the muscles and soft tissue in the graphical model and the inclusion of the biomechani-

³Part of the current thesis was developed during the COVID-19 outbreak of 2020, which imposed extraordinary measures in research facilities and experimental protocols. This prohibited experiments with external participants and considerably reduced the availability of recording equipment.

cal model dynamics for visualisation in the graphical model. Implementation of the model visualisation in the HoloLens augmented reality (AR) headset would also be desirable. Ultimately, steps towards real-time IK and motion capture, as well as patient recorded data, would entail interesting features for the project.

6 Conclusions

A successful first attempt at incorporating a musculoskeletal model into a graphical model for visualisation of the hand kinematics with medical education purposes was made. The joint pivot points and rotation axes were adjusted to match the graphical model anatomy, resulting in a good fitting between the two models, as reflected in the calculated validation metrics. This proves the feasibility of transferring the kinematics of a musculoskeletal model into a graphical model for the visualisation of hand movements, thereby creating new anatomy teaching possibilities. The current approach establishes the basis for the first accurate biomechanically-based graphical model of the hand for medical education.

Acknowledgements

I would like to thank my supervisors Dr. Ir. Winfred Mugge, Dr. Beerend P. Hierck, Katja Bogomolova, Ir. Jinne Geelen, Prof. Dr. Frans C.T. van der Helm, and Prof. Dr. Steven Hovius, for giving me the possibility of setting the start of such a long-term project. I sincerely appreciate the time invested and their encouraging attitude. I would also like to thank my family and friends for their unconditional support during these years. I especially want to thank Pedro Zufiria, Alejandro del Valle, Elisa Anderson, Alberto Gancedo and Miquel Piris for their support during the difficult stages of this thesis, as well as Pier de Jong, for his support during the writing part of the thesis.

Appendix A: Anatomical differences between the musculoskeletal model and the graphical model

The anatomical differences between the cadavers from which the musculoskeletal and graphical models

Table 4: Angle difference in the transversal orientation of the finger joints between he unscaled musculoskeletal model and the graphical model.

	MCP1	IP1	PIP2	DIP2
Angle difference	45.58°	37.13°	10.46°	15.05°

were generated imposed several limitations on the approach presented in this paper. These differences between the two models anatomy were measured based on the available landmarks for the musculoskeletal model.

CMC1 and MCP2 joints: lack of orientation correction of joint pivot points and visual adjustment of the resting pose

The angle accounting for the dimensions of each model's palm (considered as carpals and 2nd to 5th digits) was measured as the angle between the vectors originating at the RS and pointing towards the MC1b and MC2h landmarks. These measures were calculated for the unscaled musculoskeletal model (24.45°) and for the graphical model (33.15°). The angle of the graphical model is 8.69° wider than that of the musculoskeletal model, which implies larger palm dimensions in the former. This reflects on a larger distance between the starting point of the two fingers (MC1b and MC2h landmarks), as well as influencing the automated correction of the resting pose for these joints. When the angles between the corresponding proximal and distal segments to these two joints in the graphical model are set to match those of the musculoskeletal model, dissimilar visual results are obtained between models. This is caused by the palm's angle difference, which affects the pointing direction of the two distal segments (MC1 and PP2). This in turn generates erroneous results, even when the angle between the corresponding proximal and distal segments to the joints CMC1 and MCP2 is the same in the two models. To attain a similar resting pose in the two models, the CMC1 and MCP2 joint angles needed to be manually adjusted to counteract the difference in the palm's anatomy.

The differences in the transversal orientation of the joints MCP1, IP1, PIP2 and DIP2 between the two models are reported in Table 4. The fact that these differences are not constant among the joints of the same finger implies variability in the fingers configuration between the two models that could influence the correction of the resting pose of the graphical model.

Movement reproducibility of the scaled musculoskeletal model by the graphical model

The cause of the mismatch between the simulated motion using the scaled musculoskeletal model and the graphical model outcome is the built up of the anatomical differences between the two models. These can be observed in the different finger proportions reported in Table 5. The 2nd metacarpal of the graphical model appears to be larger than that of the scaled musculoskeletal model, as the ratio of the entire finger's length suggests. This, in combination with a wider palm's angle (difference of 7.98°), implies that the MCP2 and CMC1 joints of the graphical model are further away, which influences the fingertip distance at the starting pose. In

Table 5: Anatomical differences between the scaled musculoskeletal model and the graphical model in the corrected resting pose. Each mobile finger's length is considered as the sum of the lengths of the three phalanges in the case of the index, and the metacarpal and the two phalanges in the case of the thumb. The entire finger's length accounts, in addition to the mobile part, for the length between the RS and the MC1b for the case of the index and between the RS and the MC1b for the thumb.

	Scaled musc. model	Graphical model
Mobile index length /		
mobile thumb length	0.9377	1.0807
Entire index length /		
entire thumb length	1.3020	1.5272
PP2 length /		
mobile index length	0.4988	0.5488
MP2 length /		
mobile index length	0.2790	0.2717
DP2 length /		
mobile index length	0.2222	0.1795
MC1 length /		
mobile thumb length	0.3517	0.4282
PP1 length /		
mobile thumb length	0.3449	0.3735
DP1 length /		
mobile thumb length	0.3034	0.1983
Hand palm angle	25.17°	33.15°

addition to this, the differences in the proportions of the fingers when considering the individual segments' ratios produce different fingertip locations when setting all the joints' angles to the same values in the two models.

Appendix B: Analysis of the errors during scaling, computation of the static pose and inverse kinematics simulation

The marker errors arising during the scaling process and the computation of the model's static pose to fit the experimental data originate from two sources. These are the use of a reduced marker set (less than three non-collinear markers per segment) for the motion capture recordings, and certain differences in joint rotation axes between the musculoskeletal model and the experimental data that can be inferred from the position of the markers.

The limitations imposed by the motion capture system on the number and size of the markers difficult the fitting of the musculoskeletal model to the experimentally recorded movements during the IK simulation.

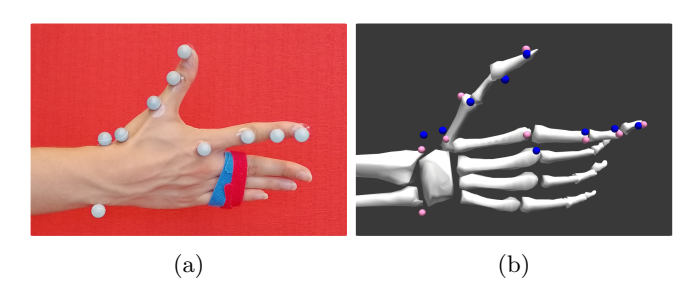


Figure 8: Scaled musculoskeletal model and participant's hand attaining the initial pose of a pinch task. The photograph in (a) was taken after performing the recordings and does not correspond to the same experimental data set used in (b). It is provided to visually aid in the explanation of the orientation mismatch. The pink markers in (b) are the virtual markers, placed in the original anatomical landmarks of the scaled musculoskeletal model. The blue markers correspond to the experimental data set.

This is considered as the main shortcoming of the approach to reproduce the experimental motion. Additionally, some differences in the rotation axes of the CMC1 joint were identified from visual inspection of the model and the marker data set. Nonetheless, these conclusions could be influenced by the aforementioned limitations in the marker set, thus additional recordings are needed before definitive conclusions about the musculoskeletal model definition can be withdrawn.

In Figure 8, it can be seen that at the initial pose of a pinch task, the experimental markers placed in the thumb are located on the dorsal side of the hand, both in the recorded marker data set (blue markers) and in the participant's hand. These markers should be coincident with the virtual markers representing the anatomical landmarks of the musculoskeletal model after scaling and setting of the static pose. Nevertheless, as it can be appreciated in Figure 8, these are located towards the lateral side of the hand. This indicates that the model is not reproducing the exact same angles at the CMC1 joint than the participant's hand. It was inspected by manual adjustments whether the thumb could reach this configuration, showing that the defined rotation axes of the 2 DoF CMC1 joint do not allow for the necessary rotation of the thumb to perfectly achieve the experimental configuration.

A larger set of recordings, employing a more extensive marker set, are needed in order to conclude whether the CMC1 joint of the musculoskeletal model needs to be reviewed.

References

Samy A Azer and Norm Eizenberg. Do we need dissection in an integrated problem-based learning medical course? Perceptions of first- and second-year stu-

- dents. Surgical and radiologic anatomy: SRA, 29 (2):173–180, mar 2007. ISSN 0930-1038 (Print). doi: 10.1007/s00276-007-0180-x.
- Esther M Bergman, Katinka J A H Prince, Jan Drukker, Cees P M van der Vleuten, and Albert J J A Scherpbier. How much anatomy is enough? Anatomical sciences education, 1(4):184–188, 2008. ISSN 1935-9780 (Electronic). doi: 10.1002/ase.35.
- Katerina Bogomolova, Ineke J M van der Ham, Mary E W Dankbaar, Walter W van den Broek, Steven E R Hovius, Jos A van der Hage, and Beerend P Hierck. The Effect of Stereoscopic Augmented Reality Visualization on Learning Anatomy and the Modifying Effect of Visual-Spatial Abilities: A Double-Center Randomized Controlled Trial. Anatomical sciences education, dec 2019. ISSN 1935-9780 (Electronic). doi: 10.1002/ase.1941.
- Dongmei Cui, Timothy D Wilson, Robin W Rockhold, Michael N Lehman, and James C Lynch. Evaluation of the effectiveness of 3D vascular stereoscopic models in anatomy instruction for first year medical students. Anatomical sciences education, 10(1):34–45, jan 2017. ISSN 1935-9780 (Electronic). doi: 10.1002/ase.1626.
- Scott L Delp, Frank C Anderson, Allison S Arnold, Peter Loan, Ayman Habib, Chand T John, Eran Guendelman, and Darryl G Thelen. OpenSim: opensource software to create and analyze dynamic simulations of movement. IEEE transactions on bio-medical engineering, 54(11):1940–1950, nov 2007. ISSN 0018-9294 (Print). doi: 10.1109/TBME.2007.901024.
- Richard L Drake, Jennifer M McBride, Nirusha Lachman, and Wojciech Pawlina. Medical education in the anatomical sciences: the winds of change continue to blow. Anatomical sciences education, 2(6): 253–259, 2009. ISSN 1935-9780 (Electronic). doi: 10.1002/ase.117.
- Agneta Gustus, Georg Stillfried, Judith Visser, Henrik Jörntell, and Patrick van der Smagt. Human hand modelling: kinematics, dynamics, applications.

 Biological Cybernetics, 106(11):741–755, 2012. ISSN 1432-0770. doi: 10.1007/s00422-012-0532-4. URL https://doi.org/10.1007/s00422-012-0532-4.
- Matthew Hackett and Michael Proctor. The effect of autostereoscopic holograms on anatomical knowledge: a randomised trial. Medical Education, 52(11):1147-1155, 2018. doi: 10.1111/medu.13729. URL https://onlinelibrary.wiley.com/doi/abs/10.1111/medu.13729.
- Mojtaba Mirakhorlo, Judith Visser, Benjamin Goislard de Monsabert, Frans van der Helm, Huub Maas, and Dirkjan Veeger. Anatomical parameters for musculoskeletal modeling of the hand and wrist.

- International Biomechanics, 3:40-49, jan 2016. doi: 10.1080/23335432.2016.1191373.
- Mojtaba Mirakhorlo, N Beek, Mariska Wesseling, Huub Maas, Dirkjan Veeger, and Ilse Jonkers. A musculoskeletal model of the hand and wrist: model definition and evaluation. Computer Methods in Biomechanics and Biomedical Engineering, pages 1–10, sep 2018. doi: 10.1080/10255842.2018.1490952.
- Prashant Sachdeva, Shinjiro Sueda, Susanne Bradley, Mikhail Fain, and Dinesh K Pai. Biomechanical Simulation and Control of Hands and Tendinous Systems. <u>ACM Trans. Graph.</u>, 34(4):42:1—42:10, 2015. ISSN 0730-0301. doi: 10.1145/2766987. URL http://doi.acm.org/10.1145/2766987.
- Ajay Seth, Michael Sherman, Peter Eastman, and Scott Delp. Minimal formulation of joint motion for biomechanisms. Nonlinear Dynamics, 62 (1):291–303, 2010. ISSN 1573-269X. doi: 10.1007/s11071-010-9717-3. URL https://doi.org/10.1007/s11071-010-9717-3.
- SimTK Confluence. Stanford University. Getting Started with Scaling. Evaluating your Results, a. URL https://simtk-confluence.stanford.edu: 8443/display/OpenSim/Getting+Started+with+ Scaling.
- SimTK Confluence. Stanford University. Getting Started with Inverse Kinematics. Evaluating your Results, b. URL https://simtk-confluence.stanford.edu:8443/display/OpenSim/Getting+Started+with+Inverse+Kinematics.
- SimTK Confluence. Stanford University. How Inverse Kinematics Works, c. URL https://simtk-confluence.stanford.edu:8443/display/OpenSim/How+Inverse+Kinematics+Works.
- Darryl G Thelen. Adjustment of muscle mechanics model parameters to simulate dynamic contractions in older adults. <u>Journal of biomechanical engineering</u>, 125(1):70–77, feb 2003. ISSN 0148-0731 (Print). doi: 10.1115/1.1531112.
- Winnie Tsang, Karan Singh, and Eugene Fiume. Helping Hand: An Anatomically Accurate Inverse Dynamics Solution for Unconstrained Hand Motion. In Proceedings of the 2005 ACM SIGGRAPH/Eurographics Symposium on Computer Animation, SCA '05, pages 319–328, New York, NY, USA, 2005. ACM. ISBN 1-59593-198-8. doi: 10.1145/1073368.1073414. URL http://doi.acm.org/10.1145/1073368.1073414.
- Bruce Wainman, Liliana Wolak, Giancarlo Pukas, Eric Zheng, and Geoffrey R Norman. The superiority of three-dimensional physical models to two-dimensional

- computer presentations in anatomy learning. $\underline{\text{Medical}}$ $\underline{\text{education}}$, 52(11):1138–1146, nov 2018. ISSN 1365-2923 (Electronic). doi: 10.1111/medu.13683.
- S W Waterston and I J Stewart. Survey of clinicians' attitudes to the anatomical teaching and knowledge of medical students. Clinical anatomy (New York, N.Y.), 18(5):380–384, jul 2005. ISSN 0897-3806 (Print). doi: 10.1002/ca.20101.